Coherent control of ultrafast bond making and subsequent molecular dynamics: demonstration of final-state branching ratio control

IOP Publishing Journal of Physics B: Atomic, Molecular and Optical Physics
J. Phys. B: At. Mol. Opt. Phys. **54** (2021) 144007 (7pp) https://doi.org/10.1088/1361-6455/ac132a

Coherent control of ultrafast bond making and subsequent molecular dynamics: demonstration of final-state branching ratio control

Liat Levin[1], Daniel M Reich[2], Moran Geva[1], Ronnie Kosloff[3], Christiane P Koch[2] and Zohar Amitay[1,*]

[1] The Shirlee Jacobs Femtosecond Laser Research Laboratory, Schulich Faculty of Chemistry, Technion-Israel Institute of Technology, Haifa 32000, Israel
[2] Dahlem Center of Complex Quantum Systems, Department of Physics, Freie Universität Berlin, Berlin, Germany
[3] Fritz Haber Research Centre, The Institute of Chemistry, Hebrew University, Jerusalem 91904, Israel

E-mail: amitayz@technion.ac.il

Received 29 April 2021, revised 3 July 2021
Accepted for publication 9 July 2021
Published 18 August 2021

Abstract

Quantum coherent control of ultrafast bond making and the subsequent molecular dynamics is crucial for the realization of a new photochemistry, where a shaped laser field is actively driving the chemical system in a coherent way from the thermal initial state of the reactants to the final state of the desired products. We demonstrate here coherent control over the relative yields of Mg_2 molecules that are generated via photoassociation and subsequently photodriven into different groups of final states. The strong-field process involves non-resonant multiphoton femtosecond photoassociation of a pair of thermally hot magnesium atoms into a bound Mg_2 molecule and subsequent molecular dynamics on electronically excited states. The branching-ratio control is achieved with linearly chirped laser pulses, utilizing the different chirp dependence that various groups of final molecular states display for their post-pulse population. Our joint experimental and theoretical study establishes the feasibility of high degree coherent control over quantum molecular dynamics that is initiated by femtosecond photoassociation of thermal atoms.

Keywords: coherent control, femtosecond coherent control, quantum coherent control, coherent control of bond making, ultrafast bond making

(Some figures may appear in colour only in the online journal)

A driving force for the field of quantum coherent control has been the idea of generating a new type of photochemistry [1–4] in which a shaped laser field actively drives the irradiated quantum system in a coherent way from the initial state of the reactants to the final state of the desired products. This is conceptually different from the common photochemistry approach, where the reactants are individually photo-excited and then react without further interaction with external fields. The key tool for the coherent control of binary reactions are shaped femtosecond laser pulses [5]. Typically, coherent control of a binary reaction proceeds in several steps. First, ultrafast coherent bond making (i.e. free-to-bound femtosecond photoassociation) is photo-induced between the free colliding reactants, and an excited bound molecule is generated. Then, subsequent photo-control over the molecular dynamics directs

* Author to whom any correspondence should be addressed.

the system into target intermediate states. Last, these intermediate states serve as a platform for further coherent photocontrol in order to selectively break bonds (i.e. femtosecond photodissociation) for generating the desired products.

Despite the significance, there is still no realization of this full scheme of binary reaction control from reactants to products. A major reason is the lack of successful coherent control of ultrafast bond making and the subsequent molecular dynamics. For binary gas phase photo-reactions where the reaction mechanism is most easily unraveled, such control has been demonstrated so far only in a few studies we have conducted [6–9]. Control of photoassociation was also demonstrated at ultralow temperatures with a timescale five orders of magnitude longer [10–13]. Quantum control of bond formation was also observed in laser-induced catalytic surface reactions [14, 15] without, however, full insight into the reaction mechanism. The key element is distillation of an entangled pair from a thermal ensemble. In strong contrast, many studies have successfully demonstrated photodissociation control of bound molecules, controlling both the total yield of fragments as well as their branching ratio to different channels [16–25].

The strong-field process in our previous photoassociation investigations [6–9] involves non-resonant multiphoton femtosecond photoassociation of a pair of thermally hot magnesium atoms into a bound excited Mg_2 molecule and subsequent molecular dynamics on electronically excited states. At the first stage, we have demonstrated the generation of purity and rovibrational coherence in the ensemble of photoassociated Mg_2 molecules via the mechanism of Franck–Condon filtering [6, 7]. Then, we have utilized the generated purity and coherence to demonstrate coherent control over the resulting yield of molecules populating a single group of final states [8, 9]. The molecular yield was enhanced with linearly-chirped femtosecond pulses having a positive chirp, reaching a maximum with a specific optimal chirp value, as well as with positively chirped pulses split into sub-pulses with a temporal structure that fits the photo-induced coherent vibrational dynamics. The different excitation and control mechanisms have been qualitatively explained by our *ab initio* calculations.

In view of controlling the full scheme of a binary reaction from reactants to products, the main limitation of our previously demonstrated bond-making control has been the control target, i.e. the overall molecular yield [6–9]. Here, we extend our approach to coherently controlling the relative yields of molecules that are generated via photoassociation and subsequently photo-driven into multiple groups of final states. The investigated ultrafast strong-field process is, as before, photoassociation of thermal magnesium atoms followed by excited-state dynamics of the generated Mg_2 molecules. The demonstrated branching-ratio control is achieved with linearly-chirped pulses, utilizing the different chirp dependence that different groups of final molecular states display for their post-pulse population. Our results establish the feasibility of high degree coherent control over quantum molecular dynamics that is initiated by femtosecond photoassociation of thermal atoms.

Figure 1 shows the potential energy curves for the magnesium dimer [7–9] together with the ultrafast excitation scheme. The starting point is an ensemble of magnesium atoms at a temperature of 1000 K that thermally populates scattering states above the van-der-Waals ground electronic state $X^1\Sigma_g^+$ of Mg_2, indicated by gray shading in figure 1. The ensemble is irradiated with shaped femtosecond laser pulses having a central wavelength of 840 nm, a transform-limited (TL) duration of 70 fs, linear polarization, and an energy that corresponds to a TL peak intensity of 7.2×10^{12} W cm^{-2}. The pulse photo-associates pairs of magnesium atoms and generates Mg_2 molecules via a free-to-bound non-resonant two-photon transition from $X^1\Sigma_g^+$ scattering states to rovibrational states of the $^1\Pi_g$ state. The corresponding Franck–Condon window is located at short internuclear distances. Then, the pulse further induces subsequent molecular dynamics on the $^1\Pi_g$ and higher electronically excited states, resulting in a post-pulse population that spans a manifold of final molecular states. Our present objective is to control the population branching ratio among different final states of the photoassociated Mg_2 molecules that cover an extended energy band located below and above the $^1\Pi_g$ asymptote, indicated also by gray shading in figure 1. These states belong to the $A^1\Sigma_u^+$, $(1)^1\Pi_u$, $(2)^1\Pi_u$ or $(2)^1\Sigma_u^+$ electronically excited states, which are all dipole-coupled to the $^1\Pi_g$ and $X^1\Sigma_g^+$ states. The $^1\Pi_g$, $A^1\Sigma_u^+$ and $(1)^1\Pi_u$ states share the same asymptote of $Mg(^1P) + Mg(^1S)$, having with the ground-state asymptote $Mg(^1S) + Mg(^1S)$ an atomic transition energy of 35 051 cm^{-1} corresponding to a measured wavelength of $\lambda_a = 285.2$ nm. For the control, we employ linearly-chirped femtosecond laser pulses, all having the same spectrum but different spectral phase. Their spectral phase is of the form $\Phi(\omega) = \frac{1}{2}k(\omega - \omega_0)^2$, where ω is a given frequency, ω_0 the central frequency of the pulse spectrum (corresponding here to a wavelength of 840 nm) and k the linear chirp parameter. The latter (k) is the control variable. The unchirped, or TL, pulse corresponds to $k = 0$.

Experimentally, magnesium vapor with a pressure of about 5 Torr is held in a heated static cell at 1000 K with Ar buffer gas, and the sample is irradiated at 1 kHz repetition rate with the intense shaped femtosecond pulses described above. They are phase shaped using a liquid-crystal spatial light modulator [5]. The post-pulse population of the final molecular states is probed by detecting and spectrally resolving the ultraviolet (UV) radiation emitted in their spontaneous radiative decay to the ground electronic state $X^1\Sigma_g^+$. The spectral range of the detected UV emission is $\lambda_{uv,S} = 281.5$ nm to $\lambda_{uv,L} = 287.5$ nm (34 783–35 524 cm^{-1}). In the setup, the UV radiation emitted toward the laser-beam entrance to the cell is collected at a small angle from the laser-beam axis using an appropriate optical setup, spectrally resolved by a spectrometer with 0.1 nm resolution, and then intensity-measured using a time-gated camera system with a post-pulse gate of 20 ns. The spectral range and resolution of the UV emission are the major differences to our earlier studies [6–9] which measured only the total UV emission intensity integrated over the range of wavelengths longer than λ_a.

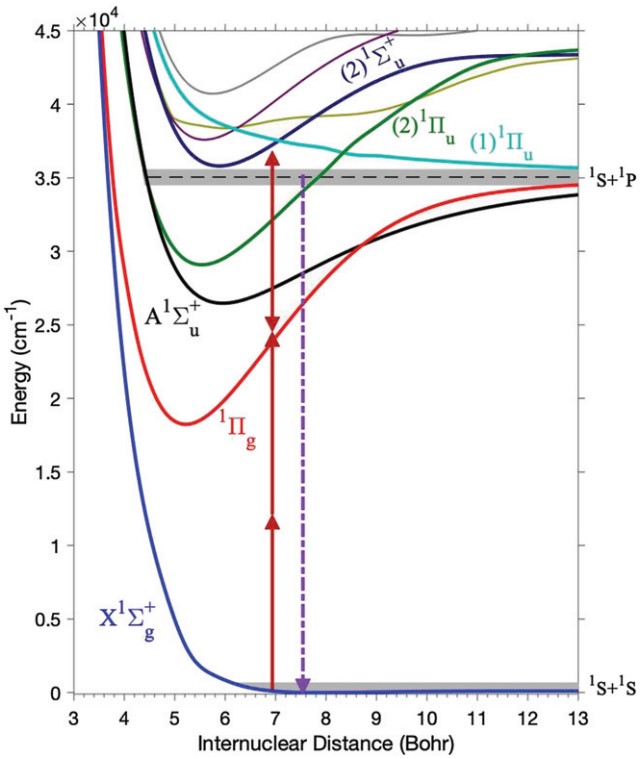

Figure 1. Potential energy curves of Mg_2 and ultrafast excitation scheme corresponding to an intense phase-shaped near-infrared linearly-polarized femtosecond pulse. The strong-field ultrafast excitation involves bond making (free-to-bound photoassociation) and subsequent molecular dynamics on the electronically excited states. The experimental observable is the spectrum of the post-pulse UV radiation spontaneously emitted from the final molecular states. The potential energy curves are plotted for the rotational quantum number $J = 70$, which corresponds roughly to the maximum of the initial thermal rotational population. The gray shades indicate the initial thermal population of scattering states and the electronically excited post-pulse population which decays by UV emission.

Figure 2 shows the experimentally measured post-pulse UV emission spectrum, obtained upon irradiation of the magnesium vapor with linearly chirped pulses. The results are presented as a color-coded map of the measured intensity, $I_{\mathrm{em}}(\lambda_{\mathrm{uv}}, k)$, as a function of the UV emission wavelength λ_{uv} and the chirp parameter k. The wavelength value of $\lambda_{\mathrm{uv}} = \lambda_{\mathrm{a}}$, corresponding to emission at the atomic transition, is indicated by a dashed black line in figure 2. Out of the full map, figure 3(a) presents examples of the measured spectrum $I_{\mathrm{em}}(\lambda_{\mathrm{uv}}; k)$ at several chirps. Figure 3(b) shows the same data normalized to the total integrated intensity $I_{\mathrm{em,tot}}(k)$, i.e. $S_{\mathrm{em}}(\lambda_{\mathrm{uv}}; k) = I_{\mathrm{em}}(\lambda_{\mathrm{uv}}; k)/I_{\mathrm{em,tot}}(k)$ with $I_{\mathrm{em,tot}}(k) = \int_{\lambda_{\mathrm{uv},S}}^{\lambda_{\mathrm{uv},L}} I_{\mathrm{em}}(\lambda_{\mathrm{uv}}; k)\mathrm{d}\lambda_{\mathrm{uv}}$ (with $\int_{\lambda_{\mathrm{uv},S}}^{\lambda_{\mathrm{uv},L}} S_{\mathrm{em}}(\lambda_{\mathrm{uv}}; k)\mathrm{d}\lambda_{\mathrm{uv}} = 1$ by definition).

As seen in figures 2 and 3, the emission spectrum $I_{\mathrm{em}}(\lambda_{\mathrm{uv}}; k)$ changes with the chirp k, such that both its shape $S_{\mathrm{em}}(\lambda_{\mathrm{uv}}; k)$ and total intensity $I_{\mathrm{em,tot}}(k)$ exhibit a strong chirp dependence. We focus here on the change in the spectral shape. The total emission results from a summation over the emission from the different final states, where each state f contributes to the total measured spectrum an individual spectrum $[I_{\mathrm{em}}^{(f)}(\lambda_{\mathrm{uv}}; k)]$ with a given state-specific shape $[S_{\mathrm{em}}^{(f)}(\lambda_{\mathrm{uv}})]$. The total intensity $[I_{\mathrm{em,tot}}^{(f)}(k)]$ for each state is proportional to the number of Mg_2 molecules populating that state $[N_{\mathrm{mol}}^{(f)}(k)]$. The corresponding proportionality constant $[\alpha_{\mathrm{em}}^{(f)}]$ depends on the different radiative channels that the state can spontaneously decay through, and stands for the intensity fraction of the state's emission at the UV spectral range detected here out of the full emission from that state. Hence, a change in the shape of the total measured spectrum $[S_{\mathrm{em}}(\lambda_{\mathrm{uv}}; k)]$ can result only from a corresponding change in the relative individual contributions of the different final states to the total spectrum. Such a change can occur due to a change in the relative population $[p^{(f)}(k) = N_{\mathrm{mol}}^{(f)}(k)/\sum_f N_{\mathrm{mol}}^{(f)}(k)]$ of multiple final states. In other words, the observed chirp-dependent changes of $S_{\mathrm{em}}(\lambda_{\mathrm{uv}}; k)$ directly imply corresponding chirp-dependent changes in the relative yields of photoassociated molecules populating the different final molecular states, i.e. coherent chirp control over the corresponding yield branching ratio.

The associated quantitative analysis is as follows. After the excitation with a pulse of chirp k, the emission spectrum from a final state f is given by $I_{\mathrm{em}}^{(f)}(\lambda_{\mathrm{uv}}; k) = \alpha_{\mathrm{em}}^{(f)} \cdot N_{\mathrm{mol}}^{(f)}(k) \cdot S_{\mathrm{em}}^{(f)}(\lambda_{\mathrm{uv}})$, such that the state-specific shape $S_{\mathrm{em}}^{(f)}(\lambda_{\mathrm{uv}})$ satisfies $\int_{\lambda_{\mathrm{uv},S}}^{\lambda_{\mathrm{uv},L}} S_{\mathrm{em}}^{(f)}(\lambda_{\mathrm{uv}})\mathrm{d}\lambda_{\mathrm{uv}} = 1$. The chirp-dependent shape of the total spectrum emitted from a group of states is then given by $S_{\mathrm{em}}(\lambda_{\mathrm{uv}}; k) = \sum_f W^{(f)}(k) \cdot S_{\mathrm{em}}^{(f)}(\lambda_{\mathrm{uv}})$ where $W^{(f)}(k) = \frac{\alpha_{\mathrm{em}}^{(f)} \cdot p^{(f)}(k)}{\sum_f \alpha_{\mathrm{em}}^{(f)} \cdot p^{(f)}(k)}$. Both $\alpha_{\mathrm{em}}^{(f)}$ and $S_{\mathrm{em}}^{(f)}(\lambda_{\mathrm{uv}})$ do not depend on the chirp k, while $p^{(f)}(k)$ might have such a dependence. Thus, indeed, the changes observed for $S_{\mathrm{em}}(\lambda_{\mathrm{uv}}; k)$ when tuning the chirp k necessarily reflect changes in the relative population $p^{(f)}(k)$ of multiple final states.

The chirp dependence of the measured emission spectrum seen in figures 2 and 3 includes several prominent characteristics. In terms of the total spectral intensity $I_{\mathrm{em,tot}}(k)$, the positively-chirped pulses enhance it with respect to the TL pulse, while the negatively-chirped pulses attenuate it. In terms of the spectral shape $S_{\mathrm{em}}(\lambda_{\mathrm{uv}}; k)$, from chirp zero up to a positive chirp k of 0.006–0.007 ps^2, it exhibits only weak chirp dependence and its dominant part is the longer-wavelength part of $\lambda_{\mathrm{uv}} > \lambda_{\mathrm{a}}$. Then, as the chirp k increases to larger positive values, the spectral shape shifts to shorter wavelengths, with an enhancement of its shorter-wavelength part and an attenuation of its longer-wavelength part. In terms of the complementary characteristic of the emission intensity $I_{\mathrm{em}}(k; \lambda_{\mathrm{uv}})$ at a given wavelength λ_{uv}, for all the detected wavelengths, it is enhanced with positively-chirped pulses over an extended range of positive chirps, and has a maximum at an emission wavelength-dependent positive chirp $k_{\mathrm{max}}(\lambda_{\mathrm{uv}})$. The value of $k_{\mathrm{max}}(\lambda_{\mathrm{uv}})$ stays unchanged (as 0.006 ps^2) for $\lambda_{\mathrm{a}} < \lambda_{\mathrm{uv}} < \lambda_{\mathrm{uv},L}$, and then continuously increases as λ_{uv} continuously decreases from λ_{a} down to $\lambda_{\mathrm{uv},S}$.

Our interpretation for the mechanism facilitating the branching-ratio control is built upon the dynamics we have previously [8, 9] identified to be induced by the positively chirped pulses. Subsequent to the $X^1\Sigma_g^+$-to-$^1\Pi_g$ free-to-bound two-photon transition, the strong-field dynamics taking place on the $^1\Pi_g$ state involves multiple resonant Raman transitions

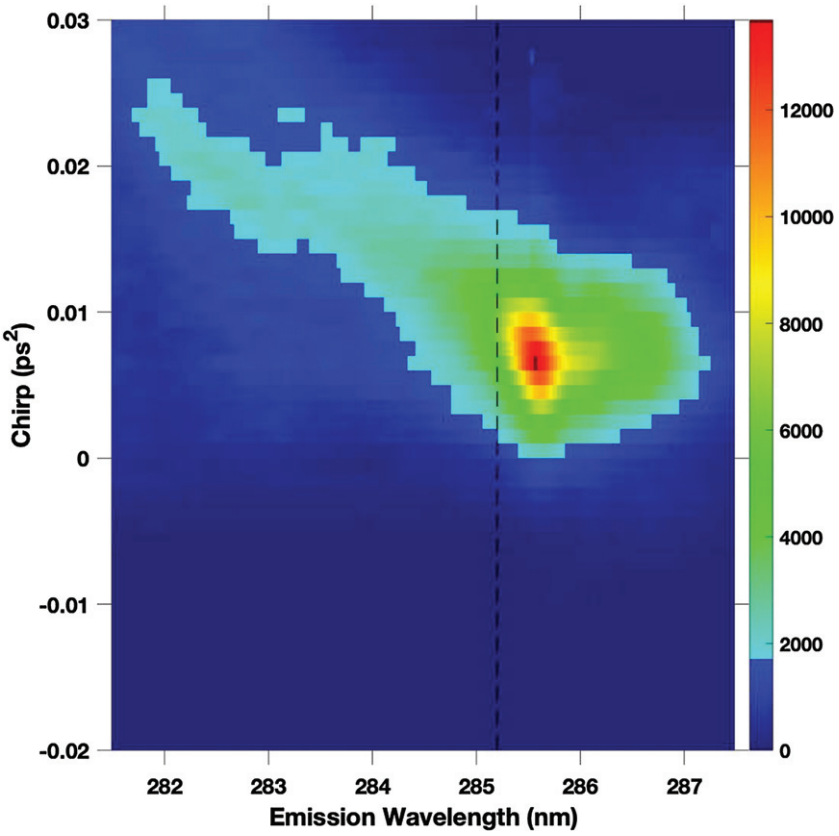

Figure 2. Experimentally detected UV emission intensity as a function of emission wavelength λ_{uv} and chirp parameter k of the linearly chirped femtosecond pulses. The intensity values are color coded, and the black dashed line indicates the wavelength λ_a corresponding to emission at the $^1\Pi_g$ atomic asymptote.

(via higher electronically excited states) that lead to a vibrational de-excitation, i.e. a population transfer into vibrational levels that are lower than the levels accessed by the photoassociative two-photon transition. Then, final perturbative one-photon absorption projects the vibrationally de-excited $^1\Pi_g$ population onto the final molecular states that emit UV light when decaying to the $X^1\Sigma_g^+$ state. The higher the energetic location of the emitting states, the higher is the energetic location of the $^1\Pi_g$ vibrational region from which they are effectively accessed by the final projection. Following their different locations, the population transfer to distinct vibrational regions is induced by a different number of Raman transitions. So, with a given pulse energy, each positively chirped pulse, due to its unique temporal intensity profile (i.e. a Gaussian of unique width), generates a different distribution of relative population among the various $^1\Pi_g$ vibrational regions and, thus, also among the various final emitting states. This, in turn, results in a different shape for the total emission spectrum $[S_{em}(\lambda_{uv};k)]$. This is the control mechanism of the present chirp-dependent branching ratio among the different final states.

Furthermore, our previous results [8] also indicate that the chirp $k_{max}^{(vib.region)}$, which maximizes the population transfer into a given $^1\Pi_g$ vibrational region, corresponds to the positively-chirped pulse having the longest temporal segment with instantaneous intensities $J_{pulse}(t)$ that are all above a certain threshold intensity $J_{th}^{(vib.region)}$. The latter is associated with the vibrational region. Increasing the chirp k from zero up to this $k_{max}^{(vib.region)}$ lengthens this segment up to a maximal duration, and a further increase in k leads to its shortening (eventually down to zero duration). For a given pulse energy, $k_{max}^{(vib.region)}$ is inversely proportional to $J_{th}^{(vib.region)}$. In other words, in order to increase the strong-field de-excitation efficiency into a specific $^1\Pi_g$ vibrational region, it is beneficial to temporally stretch the positively-chirped pulse as much as possible up to a certain limit (that depends on the vibrational-region's location). This fits the strong-field non-perturbative nature of the de-excitation dynamics. Since an efficient population transfer to a higher $^1\Pi_g$ vibrational region requires a smaller number of efficient Raman transitions, the corresponding threshold intensity $J_{th}^{(vib.region)}$ is smaller and the corresponding $k_{max}^{(vib.region)}$ is larger. As emitting states of higher excitation energy are linked with a higher vibrational region, their population and emitted radiation will thus be maximally enhanced with a larger chirp value as compared to emitting states of lower excitation energy. Hence, the present experimental chirp dependence of the total spectral shape $S_{em}(\lambda_{uv};k)$ and the emission wavelength-dependent optimal chirp $k_{max}(\lambda_{uv})$ point toward the following characteristic for the states that dominantly contribute to the detected emission: the higher the energy of the emitting state, the shorter are the UV wavelengths at which its state-specific emission spectral shape $S_{em}^{(f)}(\lambda_{uv})$ is intensified.

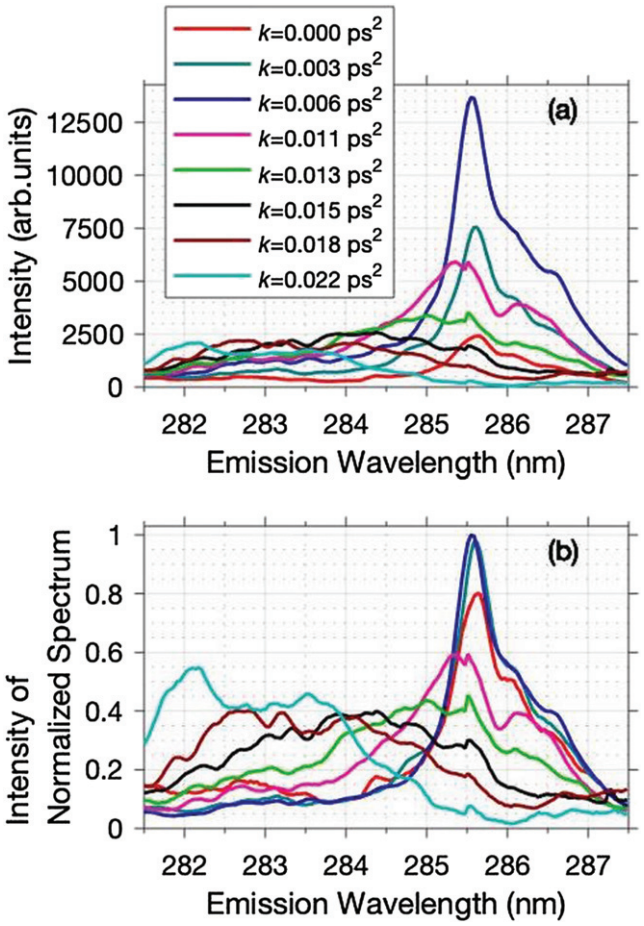

Figure 3. Examples of experimental UV emission spectra measured following the ultrafast bond-making excitation by linearly chirped femtosecond pulses for different values of the chirp parameter k. Each spectrum corresponds to a cut of the emission map of figure 2 at the corresponding chirp. For each emission spectrum, panel (a) presents the measured spectrum and panel (b) the spectral shape obtained by normalizing the measured spectrum by its total intensity. See text for details.

Considering this characteristic in combination with the results of the theoretical emission analysis described next allows us to identify the dominant emitting states.

Using the potential curves presented in figure 1 and the corresponding electronic transition dipole moments [7–9], we have assigned the origin of the experimentally detected UV emission to different electronic states and vibrational levels. First, we employ energetic considerations to group the different states according to their emission wavelength. Second, analysis of the corresponding vibrationally-averaged transition dipole moments (VTDMs) with the electronic ground state $X^1\Sigma_g^+$ allows us to calculate the full spectrum of spontaneous emission from each state in these groups. In the experimentally detected range of $\lambda_{uv,S} < \lambda_{uv} < \lambda_{uv,L}$, four such distinct sets of states can be identified: (I) high-lying vibrational levels of the $A^1\Sigma_u^+$ state near the $Mg(^1P) + Mg(^1S)$ asymptote, (II) vibrational levels of the two coupled $^1\Pi_u$ states below the $Mg(^1P) + Mg(^1S)$ asymptote, (III) vibrational levels of the two coupled $^1\Pi_u$ states above the $Mg(^1P) + Mg(^1S)$ asymptote but below the avoided crossing of the $^1\Pi_u$'s potentials, and (IV) low-to-moderately high-lying vibrational levels of the $(2)^1\Sigma_u^+$ state. States from groups (I) and (II) contribute exclusively to the emission at wavelengths longer than λ_a. States from groups (III) and (IV) contribute both to the emission at wavelengths longer and shorter than λ_a. Even though it would be energetically possible for even higher-lying states to add to the detected emission window by decaying into vibrationally high-lying levels in the electronic ground state, the VTDMs for such transitions are effectively zero. Moreover, vibrational levels on the two coupled $^1\Pi_u$ states above the avoided crossing are subject to predissociation which is rapid compared to the spontaneous-emission timescale. This implies that their contribution to UV emission can be neglected, and group (III) only contains levels below the avoided crossing.

Figure 4 shows the group-specific UV emission spectra in the experimentally detected range, calculated for rotational quantum numbers $J = 30$, 70 and 120, with $J = 70$ corresponding roughly to the maximum of the initial thermal rotational population. The results are shown as grayscale-coded maps, with each map corresponding to a different group. For each vibrational level in a group, the map shows the relative emission intensity at each wavelength assuming the initial population of the level is 100%.

A careful analysis of the calculated VTDMs and emission spectra for all rotational levels reveals that, for group (II), only very few or no vibrational levels contribute to the experimental emission window. For the example of $J = 70$ shown in figure 4, only a single contributing level remains. Furthermore, the group-specific emission intensities within the experimental emission window are larger for group (I) by two orders of magnitude as compared to all other groups. Due to the fact that group (I) only contributes to emission at wavelengths longer than λ_a, we conclude that the detected emission at this range is dominated by group (I), with several dozen vibrational levels showing large VTDM values and high emission intensities. In particular, the density of vibrational levels in group (I) is highest right below the asymptote of $Mg(^1P) + Mg(^1S)$, which leads to an accumulation of the emission intensity directly at wavelengths slightly longer than λ_a. As seen in figure 4, the identification of group (I) as dominant in the emission spectral range of $\lambda_a < \lambda_{uv} < \lambda_{uv,L}$ indeed fits the characteristic identified above for the dominant emitting states with a correlation between higher state energy and intensified emission at shorter wavelengths. Moreover, this identification of group (I) agrees with our results from previous chirp-dependent experiments and quantum dynamical calculations for the long-wavelength emission [8].

With regard to the emission at wavelengths shorter than λ_a, figure 4 shows that in this spectral range only group (III) follows the aforementioned characteristic of the dominant emitting states. Hence, we conclude that the detected emission at the spectral range of $\lambda_{uv,S} < \lambda_{uv} < \lambda_a$ is dominated by the states of group (III). This is also consistent with the larger state-specific emission intensities seen in figure 4 for group (III) as compared to group (IV). Overall, we attribute the detected emission at $\lambda_{uv} > \lambda_a$ primarily to high-lying vibrational levels of the $A^1\Sigma_u^+$ state located near the $Mg(^1P) +$

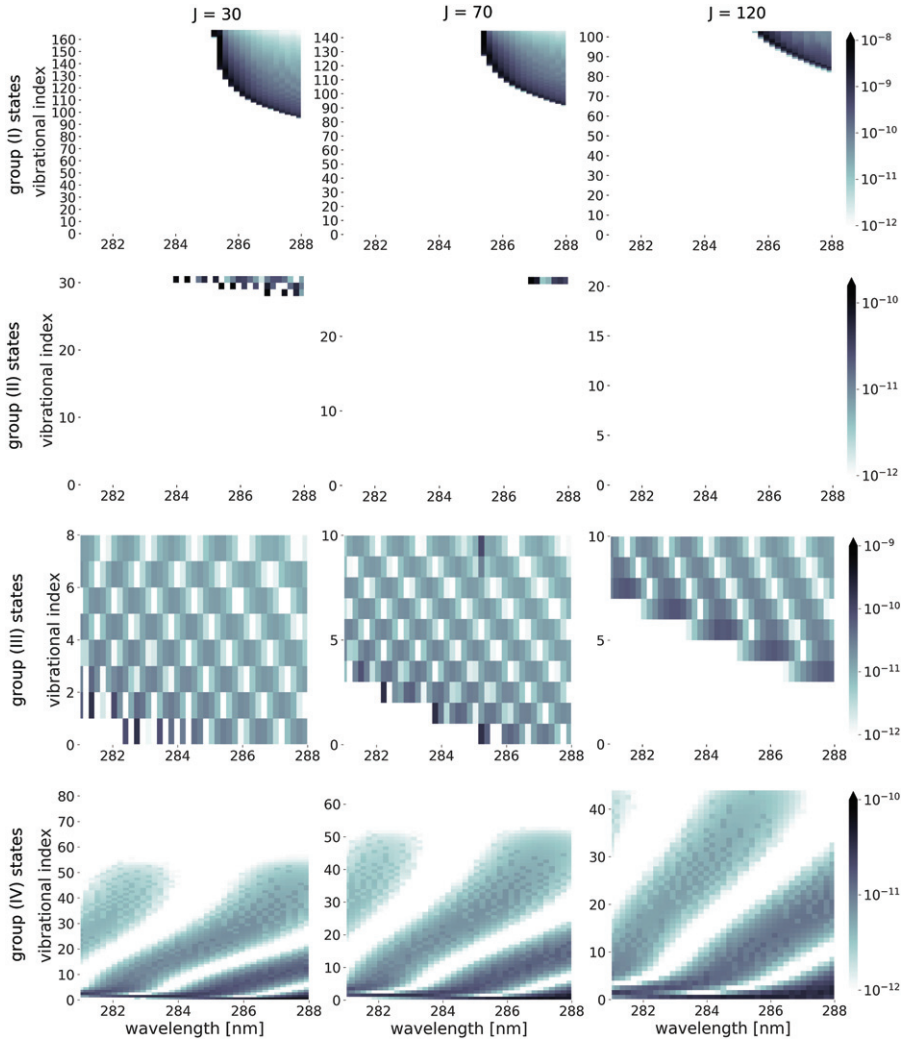

Figure 4. State-specific UV emission spectra in the experimentally detected range calculated for the vibrational levels with rotational quantum number $J = 30$, 70 and 120 that belong to the four different groups of electronically excited states which may contribute to the detected emission. Each (grayscale-coded) map corresponds to a different group, and for each vibrational level in a group, the map shows the relative emission intensity at each wavelength assuming the initial population of the level is 100%. Note the different color bar scales for the four groups.

$Mg(^1S)$ asymptote, whereas the detected emission at $\lambda_{uv} < \lambda_a$ predominantly appears to originate from vibrational levels of the two coupled $^1\Pi_u$ states located above the $Mg(^1P) + Mg(^1S)$ asymptote but below the avoided crossing.

In summary, coherent control of ultrafast bond making and subsequent molecular dynamics in experiment and theory has been extended here to demonstrating branching ratio control. The relative yields of molecules, which are coherently generated in thermal femtosecond photoassociation and subsequently photo-driven into different target states, are coherently controlled using linearly-chirped pulses of positive chirp. The control knob is the chirp of the pulse. The results are explained by calculations of the UV emission together with a model accounting for vibrational de-excitation that is photo-induced and controlled via strong-field chirped Raman transitions. Our demonstrated control is a crucial element for the realization of coherent control over the complete process of a binary photo-reaction. In the case of a reaction with several product channels, the branching ratio control to various target molecular states will be the first part of an extended scheme, in which the different target states will serve as intermediate platforms from which subsequent selective photo-control will be applied toward different product channels.

Acknowledgments

Financial support from the Deutsche Forschungsgemeinschaft (DFG—German Research Foundation) under the DFG Priority Program 1840, ‘Quantum Dynamics in Tailored Intense Fields (QUTIF)’, is gratefully acknowledged.

Data availability statement

All data that support the findings of this study are included within the article (and any supplementary files).

ORCID iDs

Ronnie Kosloff https://orcid.org/0000-0001-6201-2523
Christiane P Koch https://orcid.org/0000-0001-6285-5766
Zohar Amitay https://orcid.org/0000-0003-4434-5003

References

[1] Tannor D J and Rice S A 1985 Control of selectivity of chemical reaction via control of wave packet evolution *J. Chem. Phys.* **83** 5013–8
[2] Kosloff R, Rice S A, Gaspard P, Tersigni S and Tannor D J 1989 Wavepacket dancing: achieving chemical selectivity by shaping light pulses *Chem. Phys.* **139** 201–20
[3] Rice S A *et al* 2000 *Optical Control of Molecular Dynamics* (New York: Wiley)
[4] Shapiro M and Brumer P 2003 *Principles of the Quantum Control of Molecular Processes* (New York: Wiley-Interscience)
[5] Weiner A M 2000 Femtosecond pulse shaping using spatial light modulators *Rev. Sci. Instrum.* **71** 1929–60
[6] Rybak L, Amaran S, Levin L, Tomza M, Moszynski R, Kosloff R, Koch C P and Amitay Z 2011 Generating molecular rovibrational coherence by two-photon femtosecond photoassociation of thermally hot atoms *Phys. Rev. Lett.* **107** 273001
[7] Amaran S *et al* 2013 Femtosecond two-photon photoassociation of hot magnesium atoms: a quantum dynamical study using thermal random phase wavefunctions *J. Chem. Phys.* **139** 164124
[8] Levin L, Skomorowski W, Rybak L, Kosloff R, Koch C P and Amitay Z 2015 Coherent control of bond making *Phys. Rev. Lett.* **114** 233003
[9] Levin L, Skomorowski W, Kosloff R, Koch C P and Amitay Z 2015 Coherent control of bond making: the performance of rationally phase-shaped femtosecond laser pulses *J. Phys. B: At. Mol. Opt. Phys.* **48** 184004
[10] Carini J L, Kallush S, Kosloff R and Gould P L 2015 Enhancement of ultracold molecule formation using shaped nanosecond frequency chirps *Phys. Rev. Lett.* **115** 173003
[11] Ciamei A, Bayerle A, Chen C-C, Pasquiou B and Schreck F 2017 Efficient production of long-lived ultracold Sr_2 molecules *Phys. Rev.* A **96** 013406
[12] Blasing D B, Pérez-Ríos J, Yan Y, Dutta S, Li C-H, Zhou Q and Chen Y P 2018 Observation of quantum interference and coherent control in a photochemical reaction *Phys. Rev. Lett.* **121** 073202
[13] Kallush S, Carini J L, Gould P L and Kosloff R 2017 Directional quantum-controlled chemistry: generating aligned ultracold molecules via photoassociation *Phys. Rev.* A **96** 053613
[14] Nuernberger P, Wolpert D, Weiss H and Gerber G 2010 Femtosecond quantum control of molecular bond formation *Proc. Natl Acad. Sci.* **107** 10366–70
[15] Nuernberger P, Wolpert D, Weiss H and Gerber G 2012 Initiation and control of catalytic surface reactions with shaped femtosecond laser pulses *Phys. Chem. Chem. Phys.* **14** 1185–99
[16] Gordon R J and Rice S A 1997 Active control of the dynamics of atoms and molecules *Annu. Rev. Phys. Chem.* **48** 601–41
[17] Brixner T and Gerber G 2003 Quantum control of gas-phase and liquid-phase femtochemistry *ChemPhysChem* **4** 418–38
[18] Dantus M and Lozovoy V V 2004 Experimental coherent laser control of physicochemical processes *Chem. Rev.* **104** 1813–60
[19] Wollenhaupt M, Engel V and Baumert T 2005 Femtosecond laser photoelectron spectroscopy on atoms and small molecules: prototype studies in quantum control *Annu. Rev. Phys. Chem.* **56** 25–56
[20] Kühn O and Wöste L 2007 *Analysis and Control of Ultrafast Photoinduced Reactions* vol 87 (Berlin: Springer)
[21] Levis R J, Menkir G M and Rabitz H 2001 Selective bond dissociation and rearrangement with optimally tailored, strong-field laser pulses *Science* **292** 709–13
[22] Rabitz H, de Vivie-Riedle R, Motzkus M and Kompa K 2000 Whither the future of controlling quantum phenomena? *Science* **288** 824–8
[23] Nichols S R, Weinacht T C, Rozgonyi T and Pearson B J 2009 Strong-field phase-dependent molecular dissociation *Phys. Rev.* A **79** 043407
[24] Tóth A, Csehi A, Halász G and Vibók Á 2020 Control of photodissociation with the dynamic Stark effect induced by THz pulses *Phys. Rev. Res.* **2** 013338
[25] Iwamoto N *et al* 2020 Strong-field control of H_3^+ production from methanol dications: selecting between local and extended formation mechanisms *J. Chem. Phys.* **152** 054302